



## Land surface temperature changes in Northern Iberia since 4000 yr BP, based on $\delta^{13}\text{C}$ of speleothems

Javier Martín-Chivelet<sup>a,b,\*</sup>, M. Belén Muñoz-García<sup>a,b</sup>, R. Lawrence Edwards<sup>c</sup>,  
María J. Turrero<sup>d</sup>, Ana I. Ortega<sup>e</sup>

<sup>a</sup> Dpt. Estratigrafía, Facultad de Ciencias Geológicas, Universidad Complutense de Madrid, 28040 Madrid, Spain

<sup>b</sup> Instituto de Geociencias (CSIC-UCM), Facultad de Ciencias Geológicas, c/ José Antonio Nováis 2, 28040 Madrid, Spain

<sup>c</sup> University of Minnesota, Department of Geology and Geophysics, 310 Pillsbury Drive SE, Minneapolis, MN 55455, USA

<sup>d</sup> Ciemat, Dpt. Medioambiente, Avda. Complutense 22, 28040 Madrid, Spain

<sup>e</sup> Centro Nacional de Investigación sobre la Evolución Humana CENIEH. Paseo Sierra de Atapuerca s/n, 09002 Burgos, Spain

### ARTICLE INFO

#### Article history:

Received 9 June 2010

Accepted 14 February 2011

Available online 22 February 2011

#### Keywords:

climate change

paleoclimate

speleothem

stable isotopes

Holocene

Iberia

### ABSTRACT

The surface temperature changes for the last 4000 years in northern inland Iberia (an area particularly sensitive to climate change) are determined by a high resolution study of carbon stable isotope records of stalagmites from three caves (Kaite, Cueva del Cobre, and Cueva Mayor) separated several tens of kilometers away in N Spain. Despite the local conditions of each cave, the isotopic series show a good overall coherence, and resulted to be strongly sensitive to surface temperature changes.

The record reflects alternating warmer and colder intervals, always within a temperature range of 1.6 °C. The timing and duration of the intervals were provided by 43  $^{230}\text{Th}$ – $^{234}\text{U}$  (ICP-MS) ages. Main climatic recognized periods are: (1) 3950–3000 yr BP: warm period punctuated by cool events around ~3950, 3550 and 3250 yr BP; (2) 2850–2500 yr BP cold interval (Iron Age Cold Period); (3) 2500–1650 yr BP moderate warm period (Roman Warm Period), with maximum temperatures between 2150 and 1750 yr BP; (4) 1650–1350 yr BP cold interval (Dark Ages Cold Period), with a thermal minimum at ~1500 yr BP; (5) 1350–750 yr BP warm period (Medieval Warm Period) punctuated by two cooler events at ~1250 and ~850 yr BP; (6) 750–100 yr BP cold period (Little Ice Age) with extremes occurring at 600–500 yr BP, 350–300 yr BP, and 150–100 yr BP; and (7) the last 150 years, characterized by rapid but no linear warming (Modern Warming). Remarkably, the presented records allow direct comparison of recent warming with former warm intervals such as the Roman or the Medieval periods. That comparison reveals the 20th century as the time with highest surface temperatures of the last 4000 years for the studied area.

Spectral analysis of the time series shows consistent climatic cycles of ~400, ~900 and ~1300 yr, comparable with those recognized in the North Atlantic marine record, the Greenland ice cores, and other terrestrial records for the middle–late Holocene, suggesting common climate forcing mechanisms related to changes in solar irradiance and North Atlantic circulation patterns.

© 2011 Elsevier B.V. All rights reserved.

### 1. Introduction

Due to its privileged geographic location between the North Atlantic and the Mediterranean, the Iberian Peninsula is very sensitive to inter-annual and longer-term variations in the atmospheric circulation affecting both the North Atlantic area and the subtropical belt. Furthermore, inland Spain has been pointed out as one of the most sensible areas in Europe to the current global warming trends, as

suggested by both instrumental records (e.g., Moreno, 2005) and climate model projections for the end of the 21st century (e.g., Christensen et al., 2007; Kjellström et al., 2007). According to the models, climate change is projected to worsen conditions (higher temperatures and drought) in a region already vulnerable to climate variability, and to reduce water availability, hydropower potential, summer tourism, and crop productivity.

Despite the sensitivity of the area, there are still very few long, well-dated, and well-calibrated climate proxies that provide a broader time perspective of the changes recorded during the 20th century. These should be the basis for a better understanding of past climate variability and the basic source for calibration of paleoclimate models.

U-series dated, stable isotope series in speleothems are commonly studied in order to generate high resolution archives of climatic change. In this paper we present the  $\delta^{13}\text{C}$  record of three precisely dated

\* Corresponding author at: Universidad Complutense de Madrid, Dpt. Estratigrafía, Facultad de Ciencias Geológicas, 28040 Madrid, Spain. Tel.: +34 913944817; fax: +34 91394798.

E-mail addresses: [j.m.chivelet@geo.ucm.es](mailto:j.m.chivelet@geo.ucm.es) (J. Martín-Chivelet), [mbmunoz@geo.ucm.es](mailto:mbmunoz@geo.ucm.es) (M.B. Muñoz-García), [edwar001@umn.edu](mailto:edwar001@umn.edu) (R.L. Edwards), [mj.turrero@ciemat.es](mailto:mj.turrero@ciemat.es) (M.J. Turrero), [anaisabel.ortega@cenieh.es](mailto:anaisabel.ortega@cenieh.es) (A.I. Ortega).

speleothems that cover the last four millennia. These speleothems were retrieved from three caves in Northern Spain which show different climatic and karstic features. Despite these differences, the  $\delta^{13}\text{C}$  records of the speleothems show robust replication of their secular trends. These trends are interpreted as connected to changes in surface temperature patterns in the area at decadal to millennial scales.

**2. Study area and caves**

The study area is located in the northern part of Castilla-León, in northern Spain (Fig. 1), and comprises the landward part of the Cantabrian Ranges and the northern part of the Meseta, the high plateau that extends over large areas of inland Spain. The region is characterized by the overlap of continental and mountain climates. The precipitation is most influenced by depressions travelling eastwards from the Atlantic, particularly in autumn and winter. The Cantabrian Ranges exert a strong control in rainfall, partially isolating the area from the maritime influence and holding the warm, dry subtropical air stream during the summer months.

Three caves of this area, which have been monitored and investigated in the last years, are considered in this work: Cueva del Cobre, Kaite, and Cueva Mayor. Cueva del Cobre and Kaite are located in the southern part of the Cantabrian Ranges, whereas Cueva Mayor is situated more southward, in the northern spurs of the Meseta (Fig. 1).

Cueva del Cobre is a vast karst system developed in the Carboniferous limestones of Sierra de Peñalabra, 6 km away from the small village of Santa María de Redondo (Palencia Province). It is a water-table cave with an active low-gradient stream passage and a series of higher, relict low-gradient levels developed within 200 m of height (Rossi et al., 1997; Muñoz-García, 2007). The main entrance is located at 1620 m a.s.l. and, at this point, there are ~100 m of limestones between the main gallery and the surface. The cave is influenced by a high mountain climate. Inter-annual mean surface temperature in the cave area is 5–6 °C (Muñoz-García, 2007). Rainfall exceeds 950 mm (1990–2002 interval, Santa María de Redondo meteorological station, Agencia Estatal de Meteorología, W4°26'07" N42°59'20", 1200 m a.s.l.), and ~80% occurs during October through May. The area has a natural vegetation cover, unaffected by agriculture, which consists of high mountain grasses and bushes and small wetlands with poorly developed peat.

Kaite cave is the uppermost gallery of the Ojo Guareña Karst System (e.g., Martín-Merino, 1986), a large endokarstic complex that comprises more than 120 km of mapped galleries. It is located 18 km west to the town of Villarcayo (Burgos Province), almost at the same latitude as Cueva del Cobre, and separated from it by only 60 km (Fig. 1). Kaite is a small (~300 m), isolated, hung cavity developed on gently dipping Upper Cretaceous limestones. It is located at a height of 870 m a.s.l. and 12–18 m below the topographic surface. The measured temperature outside the cave averages 10–11 °C. Annual rainfall is ~720 mm (1990–2002 interval, Villarcayo meteorological station, Agencia Estatal de Meteorología, W3°34'20" N42°56'26", 595 m a.s.l.), with dry summer conditions. Above the cave, where a calcareous lithosol exists, the vegetation cover is defined by small xerophilous trees and bushes.

Cueva Mayor is located in the Sierra de Atapuerca, near the city of Burgos. It is one of the main conducts of the Atapuerca karst system, developed in gently dipping Cretaceous limestones. The work has been carried out in one of its secondary galleries, so-called “Galería del Sílex” (Flint Gallery), which was isolated from the entrance of the cave by a karstic collapse that occurred about 3000 years ago (Ortega, 2009). This gallery is located at a height of 1050 m a.s.l. and 12–20 m below the topographic surface (Ortega, 2009). The climate of the area is quite similar to that of Kaite area, but with a higher continental influence, with cold winters and hot summers. The mean inter-annual temperature in the area is ~10.8 °C and the annual rainfall averages 630 mm (1990–2002 interval, Atapuerca meteorological station, Agencia Estatal de Meteorología, W 3°30'27" N 42°22'35", 966 m a.s.l.), with most of the precipitation occurring between October and May (>85%). Summer conditions are usually dry, with reduced rainfall and high evapotranspiration. Above the cave, where a poor calcareous lithosol exists, the vegetation is xerophilous and consists of bushes and small trees dominated by *Quercus ilex* ssp. *rotundifoliae*, a subspecies of holm oak adapted to cold winters and dry summers.

Details on the hydrogeochemistry and environmental conditions of these caves are reported in Martín-Chivelet et al. (2006, 2008), Muñoz-García (2007), and Turrero et al. (2004, 2007). Previous work performed in stalagmites, drip waters and cave environmental conditions in the three caves indicates that calcite precipitation is taking place (and also has occurred in the past) under conditions of—or very close to—isotopic equilibrium. Specifically, this is supported by (1) positive “Hendy tests” performed on these and other stalagmites of the three caves (e.g., Martín-

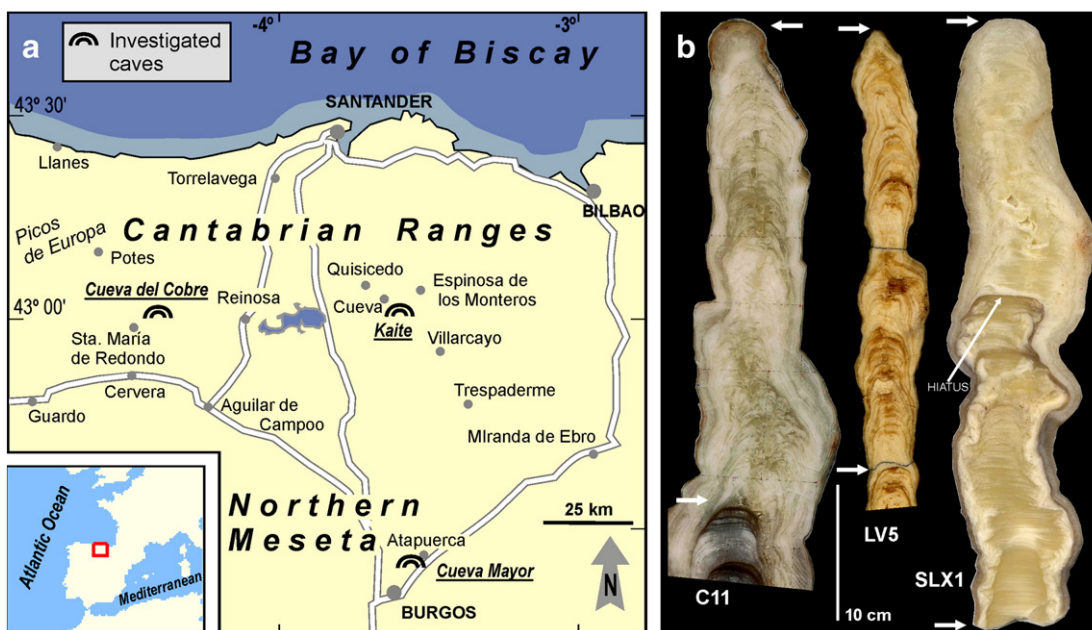


**Fig. 1.** a) Location of the three caves from which the studied stalagmites were retrieved. b) Polished longitudinal section of stalagmites C11 (Cueva del Cobre), LV5 (Kaite), and SLX1 (Cueva Mayor). The white arrows indicate the base and the top of the considered intervals (last 4000 years). The hiatus of stalagmite SLX1 is also indicated.

Chivelet et al., 2006; Muñoz-García, 2007; Domínguez-Villar et al., 2008, and unpublished data), (2) Integrated analysis of stable isotopes from present-day drip waters and calcite precipitates at the top of the stalagmites in Kaite and Cueva Mayor (the three caves (Muñoz-García, 2007; Turrero et al., 2009; Martín-Chivelet et al., 2009; and unpubl. data), and (3) Environmental analysis of sampling sites in the caves, all of them characterized by relative humidity close to 100% and the lack of significant air currents through the year. On the other hand, petrographical details on stalagmites from Cueva del Cobre are given in Muñoz-García et al. (2006, 2007) and Muñoz-García (2007); from Kaite cave in Domínguez-Villar et al. (2004, 2008) and Martín-Chivelet et al. (2006); and from Cueva Mayor-Sílex Gallery in Muñoz-García et al. (2009).

### 3. Studied material

This study is based on data from three stalagmites (Fig. 1), each of them collected in a different cave: C11 (Cueva del Cobre), SLX1 (Cueva Mayor), and LV5 (Kaite).

Stalagmite C11 was removed from Cueva del Cobre in 2002 from a small remote passage located more than 1 km away from the main entrance, an area of negligible air current, relative humidity exceeding 98%, and an air temperature nearly constant of  $5.6 \pm 0.1$  °C. The stalagmite seemed to be active when collected (it was under an active drip and presented a clean bright surface). Its total length is 30 cm and its diameter ranges between 6 and 9 cm. The sample entirely consists of columnar calcite (*sensu* Frisia et al., 2000). The growth lamination is quite irregular and is defined by differences in the density of fluid inclusions (Muñoz-García, 2007).

Stalagmite LV5 was collected from Kaite in 2002. It was fallen down and broken into several pieces when collected. The sampling site, located at 350 m from the cave entry, is characterized by stable cave climate ( $T = 10.4 \pm 0.1$  °C, relative humidity >98%, absence of significant air currents), frequent seepage, and a rich ornamentation of speleothems. LV5 is a calcite speleothem which shows dendritic, fibrous and microcrystalline fabrics (*sensu* Frisia et al., 2000) and a well defined but irregular lamination which can be interpreted as annual in origin (Domínguez-Villar et al., 2004, 2008; Martín-Chivelet et al., 2006). Its total length is ~100 cm and its diameter ranges between 3 and 6 cm. In this paper, only the upper part of the stalagmite is considered (Fig. 1).

Stalagmite SLX1 was retrieved from Galería del Sílex in Cueva Mayor. It was slightly moved from its drip point in 1990 during pioneer speleological exploration works, and latterly collected in 2002. The sampling site has no air currents, a relative humidity exceeding 99%, and a very stable temperature of  $10.6 \pm 0.1$  °C. Stalagmite SLX1 is 35 cm long and cylindrical in shape, with a diameter of 7–10 cm. The polished longitudinal section of the stalagmite shows in its middle part a well-outlined stratigraphic hiatus, marked by a darker color (Fig. 1), but no corrosion. Below and above this hiatus, the stalagmite consists of clean calcite that shows columnar, fibrous and dendritic fabrics (*sensu* Frisia et al., 2000), and contains a quite regular lamination which corresponds to annual growth layers (unpubl. data).

### 4. Methods

#### 4.1. Carbon stable isotopes

Stable isotope ratios of carbon ( $^{13}\text{C}/^{12}\text{C}$ ) were measured for a total of 520 calcite microsamples. These were extracted with carbide dental burrs of 0.5 mm directly from petrographical thin sections performed along the growth axis of the stalagmites. Typical powder masses are of ~100 µg. Spacing between samples ranged from 1 mm to 0.5 mm, depending on the growth rates. The analyses were performed in the Minnesota Isotope Laboratory using a Finnigan-MAT 252 mass spectrometer fitted with a Kiel Carbonate Device III. Duplicates were analyzed every 10 to 20 samples, all of which replicated within 0.20‰ for carbon. Values are reported as  $\delta^{13}\text{C}$  with respect to the Vienna Pee

Dee Belemnite (VPDB) standard. From those analyses, stable isotope ratios of oxygen ( $^{18}\text{O}/^{16}\text{O}$ ) were also obtained. These oxygen data, partially published elsewhere (Muñoz-García, 2007; Domínguez-Villar et al., 2008) are not considered specifically in this paper.

#### 4.2. $^{230}\text{Th}$ age-dating

Sub-samples from stalagmites LV5, SLX1, and C11 were prepared for  $^{230}\text{Th}$  dating following procedures similar to those described by Edwards et al. (1987) and Dorale et al. (2004). These were extracted from well-defined growth horizons with the aid of 0.5–0.9 mm carbide dental burrs. Typical powder amounts are 100–200 mg for C-11, 150–250 mg for SLX1, and 200–350 mg for LV5 (different amounts of sample were necessary because of the different uranium concentration in the stalagmites). Analyses were conducted in the Minnesota Isotope Laboratory of the University of Minnesota by means of inductively coupled plasma mass spectrometer (Thermo-Finnigan ELEMENT) using procedures described in Shen et al. (2002) and Dorale et al. (2004). Eleven previously published Th-age dates for stalagmite LV5 (Domínguez-Villar et al., 2008) were considered in this work, and incorporated into the age model.

#### 4.3. Complementary techniques

This study was carried out with the aid of petrographical analyses of the speleothems, which are considered essential for recognizing the internal stratigraphy of the stalagmites (e.g., identification of hiatuses and growth patterns), and also for choosing the extraction points of subsamples for absolute age-datings and stable isotope analyses. Some zones showing depositional condensation (strongly reduced growth rates), incipient recrystallization, or other diagenetic features, were discarded for performing the geochemical analyses of this research. Details on the microstratigraphical and petrographical methodology can be found in Martín-Chivelet et al. (2006) and Muñoz-García et al. (2006).

### 5. Results

#### 5.1. Age models

A total of 43  $^{230}\text{Th}$  absolute ages covering the last 4000 years were used to perform the age models of the three stalagmites. The uranium and thorium mass spectrometric results and the corresponding ages and errors are shown in Table 1.

Stalagmite C11: 10 absolute-dated ages were obtained from the 33.5 cm of core that covers the last ~2700 years. All the  $^{230}\text{Th}$  ages are in correct stratigraphic order. Petrographical analyses suggest a continuous growth for the considered time interval. The age model for this stalagmite (Fig. 2a) is based on linear interpolation between successive dated points. Calculated growth rates are essentially homogeneous through the 2700 years, averaging 124 mm/ky.

Stalagmite SLX1: 14 absolute-dated ages were obtained from this stalagmite, covering the complete core of the sample (44 cm). SLX-1 shows an important hiatal surface, easily recognizable *de visu* and in thin section, which separates two intervals of continuous growth but at different rates. The older interval ranges from ~1.6 to ~0.6 ky BP, and shows an average growth rate of 240 mm/yr; the younger one covers the last four centuries and shows notably higher growth rates, averaging 490 mm/ky. The age model for this stalagmite is based on linear interpolation between dated points excepting for those above and below the hiatus (Fig. 2b). For those, the growth rates of the adjacent intervals were considered for age interpolation.

Stalagmite LV5: 19 absolute-dated ages were obtained from the interval that covers the last four millennia. That interval corresponds to the uppermost 32 cm of the stalagmite. The  $^{230}\text{Th}$  ages are in correct stratigraphic order. No evident post-formational alteration or significant

**Table 1**  
Uranium and thorium isotopic compositions and  $^{230}\text{Th}$  ages for stalagmites C11, LV5 and SLX1 by ICP-MS.

Sample ID	Distance mm from base	$^{238}\text{U}$ ppb	$^{232}\text{Th}$ ppt	$d^{234}\text{U}$ measured <sup>a</sup>	$[\text{}^{230}\text{Th}/\text{}^{238}\text{U}]$ activity <sup>c</sup>	Age-year (uncorrected)	Age-year BP (corrected) <sup>c,d</sup>	$\delta^{234}\text{U}_{\text{initial}}$ corrected <sup>b</sup>
C11-MNE	98	621.2 ± 1.6	181 ± 3	426.3 ± 3.4	0.03467 ± 0.00031	2 678 ± 25	2 614 ± 26	429.5 ± 3.4
C11-MN02	147	512.1 ± 0.9	33 ± 4	411.7 ± 2.3	0.02942 ± 0.00041	2 293 ± 32	2 233 ± 34	414.4 ± 2.3
C11-MN03	186	543.0 ± 1.3	44 ± 4	406.8 ± 3.1	0.02566 ± 0.00035	2 004 ± 28	1 944 ± 26	409.1 ± 3.2
C11-MN04	206	555.0 ± 1.5	23 ± 3	387.4 ± 3.6	0.02220 ± 0.00028	1 756 ± 23	1 697 ± 122	389.3 ± 3.6
C11-MN05	238	587.3 ± 1.6	585 ± 5	381.5 ± 3.3	0.01932 ± 0.00036	1 534 ± 29	1 455 ± 126	383.2 ± 3.3
C11-MN06	273	693.5 ± 1.9	77 ± 3	348.0 ± 3.2	0.01650 ± 0.00028	1 341 ± 23	1 281 ± 132	349.3 ± 3.2
C11-MN07	322	543.1 ± 1.4	58 ± 4	374.0 ± 3.3	0.01050 ± 0.00022	835 ± 18	775 ± 182	374.9 ± 3.3
C11-MN08	361	567.2 ± 1.5	21 ± 3	387.1 ± 3.2	0.00674 ± 0.00020	530 ± 16	472 ± 195	387.7 ± 3.2
C11-MN09	392	543.6 ± 1.6	42 ± 4	400.8 ± 3.9	0.00465 ± 0.00023	362 ± 18	303 ± 90	401.2 ± 3.9
C11-MN10	418	508.4 ± 1.2	16 ± 3	353.4 ± 3.0	0.00169 ± 0.00015	136 ± 12	77 ± 61	353.6 ± 3.0
LV5-3CIII	743	98.4 ± 0.4	396 ± 11	148.9 ± 6.4	0.04177 ± 0.00120	4 041 ± 121	3 885 ± 131	150.6 ± 6.5
LV5-4A	768	86.7 ± 0.1	102 ± 4	147.3 ± 3.4	0.03696 ± 0.00131	3 573 ± 129	3 490 ± 130	148.8 ± 3.5
LV5-HK5	785	88.4 ± 0.2	143 ± 2	141.8 ± 3.2	0.03464 ± 0.00075	3 354 ± 74	3 255 ± 77	143.2 ± 3.2
LV5-4BI	800	93.5 ± 0.2	120 ± 3	150.3 ± 2.8	0.03172 ± 0.00084	3 052 ± 83	2 966 ± 84	151.6 ± 2.8
LV5-4BIII	819	210.7 ± 0.5	245 ± 9	162.3 ± 2.5	0.02989 ± 0.00051	2 843 ± 50	2 759 ± 52	163.6 ± 2.5
LV5-4BIV	834	158.9 ± 0.3	348 ± 6	164.8 ± 1.9	0.02906 ± 0.00039	2 757 ± 37	2 648 ± 46	166.1 ± 1.9
LV5-4BT	845	79.7 ± 0.1	128 ± 5	166.4 ± 2.3	0.02614 ± 0.00052	2 474 ± 50	2 379 ± 54	167.6 ± 2.4
LV5-HK4n	858	106.6 ± 0.3	249 ± 2	155.7 ± 3.8	0.02437 ± 0.00048	2 321 ± 47	2 204 ± 56	156.7 ± 3.8
LV5-4 C	872	148.9 ± 0.6	1378 ± 13	149.3 ± 4.7	0.02537 ± 0.00096	2 437 ± 93	2 147 ± 150	150.2 ± 4.7
LV5-HK3	906	110.5 ± 0.2	165 ± 2	150.0 ± 2.6	0.01969 ± 0.00039	1 881 ± 38	1 785 ± 43	150.8 ± 2.6
LV5-5AI	930	114.0 ± 0.2	283 ± 4	146.8 ± 2.8	0.01786 ± 0.00072	1 713 ± 69	1 597 ± 76	147.5 ± 2.8
LV5-5AII	934	109.9 ± 0.2	384 ± 4	148.7 ± 2.7	0.01747 ± 0.00078	1 673 ± 75	1 532 ± 87	149.3 ± 2.7
LV5-HK1	940	118.7 ± 0.2	240 ± 2	148.4 ± 2.4	0.01715 ± 0.00043	1 639 ± 41	1 530 ± 48	149.1 ± 2.4
LV5-HK2n	959	136.9 ± 0.3	203 ± 2	149.5 ± 2.9	0.01468 ± 0.00039	1 400 ± 38	1 304 ± 42	150 ± 3
LV5-K5A	965	105.0 ± 0.3	1664 ± 7	142.5 ± 3.8	0.01751 ± 0.00078	1 682 ± 76	1 220 ± 216	143.0 ± 3.8
LV5-5B	992	127.4 ± 0.3	475 ± 3	139.9 ± 3.6	0.01101 ± 0.00053	1 060 ± 52	912 ± 70	140.3 ± 3.6
LV5-K5C	1017	124.9 ± 0.4	719 ± 4	140.7 ± 3.5	0.01120 ± 0.00053	1 075 ± 51	870 ± 89	141.1 ± 3.5
LV5-K20	1031	136.8 ± 0.4	386 ± 4	143.8 ± 3.8	0.00981 ± 0.00057	938 ± 55	808 ± 66	144.2 ± 3.8
LV5-5 C	1038	124.7 ± 0.2	80 ± 3	148.8 ± 2.3	0.00485 ± 0.00052	462 ± 50	393 ± 50	149.0 ± 2.3
SLX1-MN01	14	132.0 ± 0.5	70 ± 2	123.4 ± 3.5	0.01622 ± 0.00045	1 584 ± 45	1 513 ± 45	124.0 ± 3.5
SLX1-MN02	45	157.5 ± 0.6	24 ± 2	122.3 ± 3.6	0.01524 ± 0.00060	1 489 ± 59	1 427 ± 59	122.8 ± 3.6
SLX1-MN03	65	149.7 ± 0.5	45 ± 1	119.6 ± 4.0	0.01459 ± 0.00060	1 429 ± 59	1 363 ± 59	120.1 ± 4.0
SLX1-MN05B	115	79.0 ± 0.3	185 ± 2	130.4 ± 4.2	0.01364 ± 0.00057	1 322 ± 56	1 204 ± 63	130.8 ± 4.2
SLX1-MN05C	165	73.5 ± 0.3	85 ± 2	130.7 ± 4.9	0.01254 ± 0.00065	1 214 ± 64	1 126 ± 65	131.2 ± 4.9
SLX1-MN06	189	123.5 ± 0.5	449 ± 3	125.2 ± 4.8	0.01111 ± 0.00075	1 081 ± 74	929 ± 87	125.5 ± 4.8
SLX1-MN06B	201	100.7 ± 0.4	49 ± 1	126.2 ± 4.7	0.00923 ± 0.00038	896 ± 37	825 ± 38	126.5 ± 4.7
SLX1-MN07	220	79.7 ± 0.4	291 ± 3	119.6 ± 7.0	0.00840 ± 0.00106	820 ± 104	667 ± 114	119.9 ± 7.1
SLX1-MN07B	228	94.3 ± 0.4	982 ± 4	120.0 ± 5.2	0.00673 ± 0.00053	657 ± 52	328 ± 145	120.1 ± 5.2
SLX1-MN09	249	79.0 ± 0.2	138 ± 1	123.6 ± 3.0	0.00339 ± 0.00033	329 ± 39	226 ± 39	123.7 ± 3.0
SLX1-MN08B	283	50.4 ± 0.2	243 ± 2	108.8 ± 6.4	0.00397 ± 0.00065	391 ± 64	206 ± 90	108.8 ± 6.4
SLX1-MN10B	340	52.1 ± 0.2	125 ± 1	114.2 ± 4.2	0.00207 ± 0.00052	202 ± 51	81 ± 60	114.2 ± 4.2
SLX1-MN12	356	50.2 ± 0.1	13 ± 1	124.5 ± 3.9	0.00185 ± 0.00041	179 ± 40	115 ± 40	124.6 ± 3.9
SLX1-MN14	412	55.7 ± 0.2	38 ± 1	126.4 ± 7.2	0.00064 ± 0.00092	62 ± 89	−14 ± 89	126.4 ± 7.2

Analytical errors are 2σ of the mean.

<sup>a</sup> $d^{234}\text{U} = ([\text{}^{234}\text{U}/\text{}^{238}\text{U}]_{\text{activity}} - 1) \times 1000$ .

<sup>b</sup> $\delta^{234}\text{U}_{\text{initial}}$  corrected was calculated based on  $^{230}\text{Th}$  age (T), i.e.,  $\delta^{234}\text{U}_{\text{initial}} = \delta^{234}\text{U}_{\text{measured}} \times e^{\lambda^{234}\text{T}}$ , and T is corrected age.

<sup>c</sup> $[\text{}^{230}\text{Th}/\text{}^{238}\text{U}]_{\text{activity}} = 1 - e^{-\lambda^{230}\text{T}} + (\delta^{234}\text{U}_{\text{measured}}/1000)[\lambda^{230}/(\lambda^{230} - \lambda^{234})](1 - e^{-(\lambda^{230} - \lambda^{234})\text{T}})$ , where T is the age.

Decay constants are  $9.1788 \times 10^{-6} \text{ yr}^{-1}$  for  $^{230}\text{Th}$ ,  $2.8263 \times 10^{-6} \text{ yr}^{-1}$  for  $^{234}\text{U}$ , and  $1.55125 \times 10^{-10} \text{ yr}^{-1}$  for  $^{238}\text{U}$  (Cheng et al., 2000).

<sup>d</sup>Age corrections were calculated using an average crustal  $^{230}\text{Th}/^{232}\text{Th}$  atomic ratio of  $4.4 \times 10^{-6} \pm 2.2 \times 10^{-6}$ .

Those are the values for a material at secular equilibrium, with the crustal  $^{232}\text{Th}/^{238}\text{U}$  value of 3.8. The errors are arbitrarily assumed to be 50%.

hiatuses were observed under the microscope. Again, for constructing the age model, continuous and homogeneous growth was considered between two successive absolute-dated points (Fig. 2c). The model reveals slightly variable growth rates, which average 88 mm/ky.

## 5.2. $\delta^{13}\text{C}$ speleothem series

The  $\delta^{13}\text{C}$  VPDB values notably vary through the growth axis of the three stalagmites, showing well-defined intervals and trends in each sample (Fig. 3). Some parts of the records seem to show cyclic patterns, and spectral analyses were performed for each stalagmite. These were based on the Lomb periodogram algorithm, indicated for unevenly spaced time series, and performed with the aid of software PAST (Hammer et al., 2003).

Stalagmite C11:  $\delta^{13}\text{C}$  values range from −6.6 to −2.3‰, with an average of −4.5‰ and a standard deviation of 1.0‰. The time series does not show any significant trend for the whole record, but several time intervals are characterized by well-defined patterns (Fig. 3). The spectral

diagram for the series (Fig. 4a) shows a significant peak at a period of ~900 yr, and a weaker peak around ~90 yr, with a significance level close to 0.01.

Stalagmite SLX1: Its isotopic record ranges from −12.1 to −7.2‰. The average is −10.3‰ and the standard deviation is 0.9‰. The two growth intervals of this stalagmite show a broad positive trend ( $\delta^{13}\text{C}$  increases with time), which is greater in the younger one (Fig. 3). Given the short length (1500 years) and the incompleteness of the record (hiatus between 650 and 350 yr BP) the spectral analysis was performed only for the older growth interval (Fig. 4b). It yields two higher frequency significant peaks at periods of ~440 yr and ~230 yr.

Stalagmite LV5:  $\delta^{13}\text{C}$  values vary from −11.2 to −5.0‰, averaging −8.7‰ and showing a standard deviation of 1.2‰. In this stalagmite, the  $\delta^{13}\text{C}$  time series does not show a consistent general pattern. Instead, several intervals showing well-defined trends can be differentiated (Fig. 3). The spectral analysis (Fig. 4c) shows four peaks with a significance level greater than 0.01, which correspond respectively to periods of ~1300, 920, 680 and 430 yr.

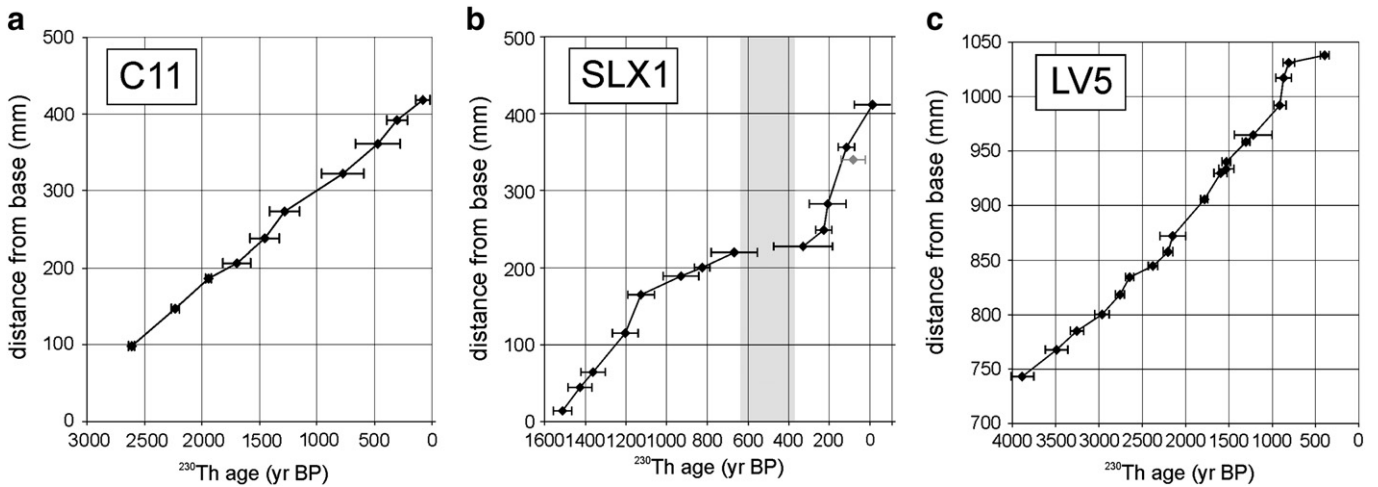


**Fig. 2.** Age models for stalagmites C11 (Cueva del Cobre), LV5 (Kaite), and SLX1 (Cueva Mayor). The models are based on linear interpolation between successive dated points ( $^{230}\text{Th}$  ages are shown in Table 1).

The basic statistical results for the  $\delta^{13}\text{C}$  records of the intervals of simultaneous growth in the three stalagmites are summarized in Table 2. Notable differences in the mean values of  $\delta^{13}\text{C}$  in each stalagmite can be appreciated. Stalagmite C11 shows 3.7‰ heavier values than LV5 and 5.6‰ than SLX1, a difference that should be related with the different physicochemical features of each cave (see interpretation below). Differences in the standard deviation are less significant, indicating that the  $\delta^{13}\text{C}$  in each stalagmite varies within a relatively similar range. Table 2 also includes the main periods recognized in the spectral diagrams. An interesting aspect is the

coincidence of some periods defining cycles in the records, despite their different length and completeness.

**6. Interpretation**

*6.1. Climate calibration of  $\delta^{13}\text{C}$  records*

Interpretation of speleothem  $\delta^{13}\text{C}$  series in terms of paleoclimate variability is not a straightforward task, as multiple factors can potentially control or affect the records (see McDermott, 2004; Fairchild

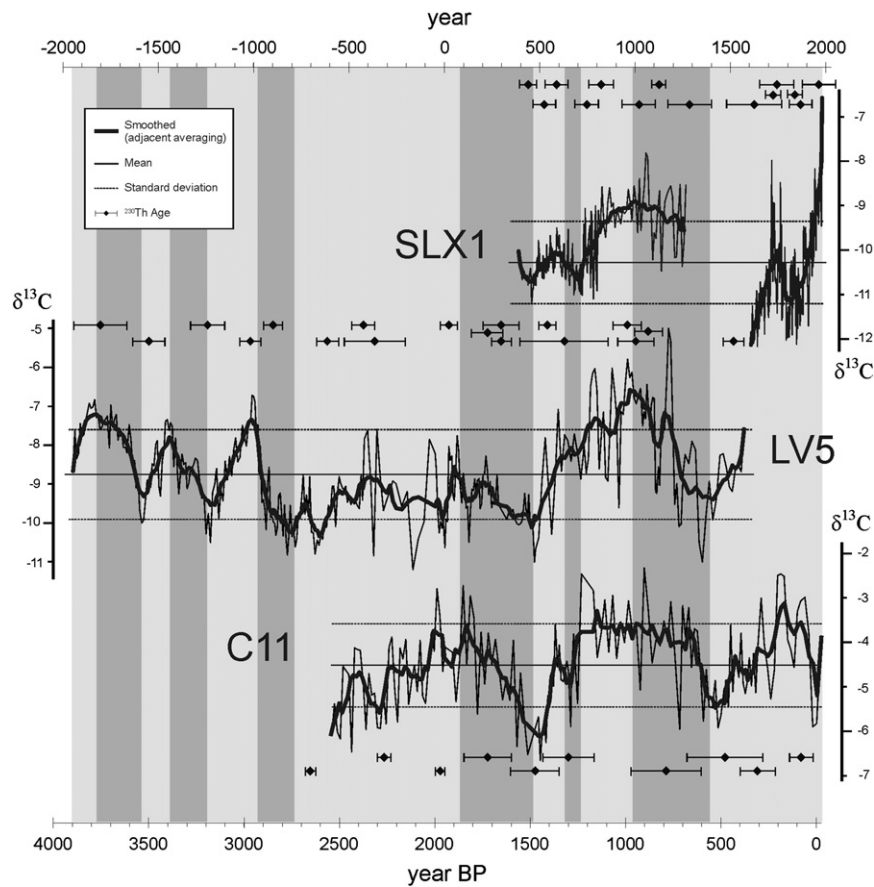


**Fig. 3.**  $\delta^{13}\text{C}$  VPDB time series for stalagmites C11 (Cueva del Cobre), LV5 (Kaite), and SLX1 (Cueva Mayor). Gray-shaded areas define intervals of dominant positive or negative trends in the three records.  $^{230}\text{Th}$  ages and  $2\sigma$  errors are also shown in the series.

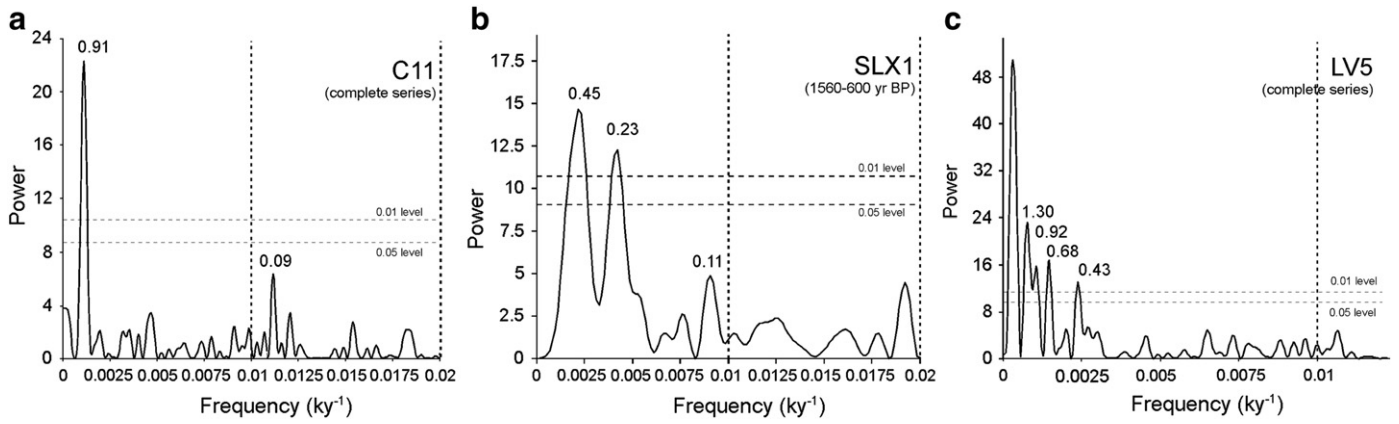


**Fig. 4.** Spectral diagrams performed for the  $\delta^{13}\text{C}$  series of a) Stalagmite C11, b) Stalagmite SLX1, and c) Stalagmite LV5. Spectral analyses were performed with the Lomb periodogram algorithm, indicated for unevenly spaced time series, and with PAST software (Hammer et al., 2003). Numbers labelled in the diagrams indicate periodicities (in ky) of the main spectral peaks.

et al., 2006; McDermott et al., 2006 for reviews, and the discussion below). In this paper, the approach has been: (1) to analyze and compare the  $\delta^{13}\text{C}$  time series of the three stalagmites, (2) to compare the youngest part of the series with instrumental series of the main climatic parameters—temperature and precipitation, and (3) to correlate the record of the last millennium with the available reconstructed paleoclimate series.

The spiky nature of the stable isotope signal determines that trends and medium-term patterns in the series are usually much more meaningful than single values. The direct comparison among the curves reveals notable coincidences in the three records (Fig. 3). In fact, they replicate a series of intervals of positive trend (increasing values of  $\delta^{13}\text{C}$  with time; marked in light grey pattern), as well as others of negative trend (decreasing values, marked with a darker grey), and the main shifts and peaks. This good, overall correlation strongly suggests a common mechanism controlling the  $\delta^{13}\text{C}$  records despite the notable differences among the karst systems and the different features of the stalagmites. This common mechanism should be external to the karst systems and thus probably related to climate.

The most recent part of the  $\delta^{13}\text{C}$  series from SLX1 (the stalagmite with the most precise and complete record for the last centuries) has been compared with the instrumental records of temperature and rainfall available for Burgos, located only 14 km away from Cueva Mayor (Fig. 5a). The used series correspond to annual and summer rainfall in Burgos (data retrieved from the Global Historical Climatology Network-US National Climatic Data Center); the annual mean temperature in Burgos (data from the Agencia Nacional de Meteorología, Spain) completed with historical instrumental data from Madrid (Almarza, 2000; Carreras, 2001); and the summer potential evapotranspiration

(PET), calculated by means of Thornthwaite's method (Thornthwaite, 1948). These records, based on instrumental data, indicate a net non-linear increase in the mean annual temperature of  $\sim 1.5\text{--}2\text{ }^\circ\text{C}$  (similar to other inland records in central and northern Spain, e.g., Raso, 1997), but do not show a clear trend in annual and summer rainfall changes. As can be expected, the summer PET series also show a net increase through the 20th century, reflecting the temperature increase.

The positive trend showed for the last 125 years in the  $\delta^{13}\text{C}$  record of stalagmite SLX1 can be correlated with the net increase along this interval in annual temperature and summer PET (Fig. 5a). On the contrary, no evident correlation with rainfall patterns can be recognized for this interval. This suggests that temperature rather than precipitation is a main control factor of  $\delta^{13}\text{C}$  variability of the studied speleothems.

The positive correlation between speleothem  $\delta^{13}\text{C}$  values and surface temperature is also robust when considering longer intervals. Available reconstructed paleotemperature series for the Northern Hemisphere for both the last four centuries (e.g., Mann and Jones, 2003) and the last two millennia (Mann et al., 2008) show very similar patterns to those outlined by the speleothem records (Fig. 5b and c respectively).

Despite the broad good correlation between surface temperatures and speleothem  $\delta^{13}\text{C}$ , establishing precise transfer functions between  $\delta^{13}\text{C}$  and temperature is a difficult task. This is mainly due to the incomplete nature of the record and the uncertainties associated to microsampling (each microsample can represent the average composition of  $\delta^{13}\text{C}$  of several years) and age-dating (we can assume an arbitrary error of  $\pm 5$  years for the last 150 years in stalagmite SLX1). As a tentative approach, we have included a correlation cross-plot (Fig. 6) between instrumental record of temperatures in Burgos area for the interval 1875–2000 (the series represented in Fig. 5a) and  $\delta^{13}\text{C}$  values of the time-equivalent interval of SLX1. The temperature values in the cross-plot are ten-year averages of the annual mean temperatures.

The cross-plot shows the results of a linear fit model for describing the relationship between  $\delta^{13}\text{C}$  and temperature. The equation of the model [ $T\text{ (}^\circ\text{C)} = 11.51 + 0.198 * \delta^{13}\text{C (}\text{‰})$ ] gives essentially  $\sim 0.2\text{ }^\circ\text{C}$  of temperature increase per unit (‰) of increment in  $\delta^{13}\text{C}$ . The  $R^2$  reaches 0.41 (i.e. the model explains the 41% of the variability in the temperatures), and the Correlation Coefficient equals 0.64, indicating a moderately strong relationship between the two variables. The standard error (given by the standard deviation of the residuals) is 0.26. This value will be used to determine the limits of temperature estimations obtained from the  $\delta^{13}\text{C}$  series.

It should be noted that this linear model fit must be considered as a first empirical approximation. Further  $\delta^{13}\text{C}$  series from recent speleothems in the area should contribute to develop more accurate transfer functions between the proxy values and the surface temperatures.

**Table 2**  
Comparative results for the  $\delta^{13}\text{C}$  records of stalagmites C11 (Cueva del Cobre), LV5 (Kaité) and SLX1 (Cueva Mayor).

	C11	LV5	SLX1
$\delta^{13}\text{C}$ —mean <sup>(a)</sup>	−4.53	−8.73	−10.28
$\delta^{13}\text{C}$ —mean <sup>(b)</sup>	−4.39	−8.07	−10.01
Standard deviation <sup>(a)</sup>	0.97	1.16	0.91
Cave temperature $^\circ\text{C}$ <sup>(c)</sup>	5.5	10.4	10.6
Cave depth <sup>(c)</sup>	~100 m	14 m	20 m
$\delta^{13}\text{C}$ —host rock <sup>(d)</sup>	−3.5–4.5	−1.5–2.5	~1.5–2.0
Spectral peaks (Period—ky)	0.91, 0.09	1.30, 0.92, 0.68, 0.43	0.44, 0.23, 0.11

(a) For all the data of each series.  
 (b) For the interval of coeval growth in the 3 stalagmites (1570–670 yr BP).  
 (c) At the sampling site.  
 (d) Average values for Carboniferous (C11) and Cretaceous (LV5, SLX1) rocks above the caves.

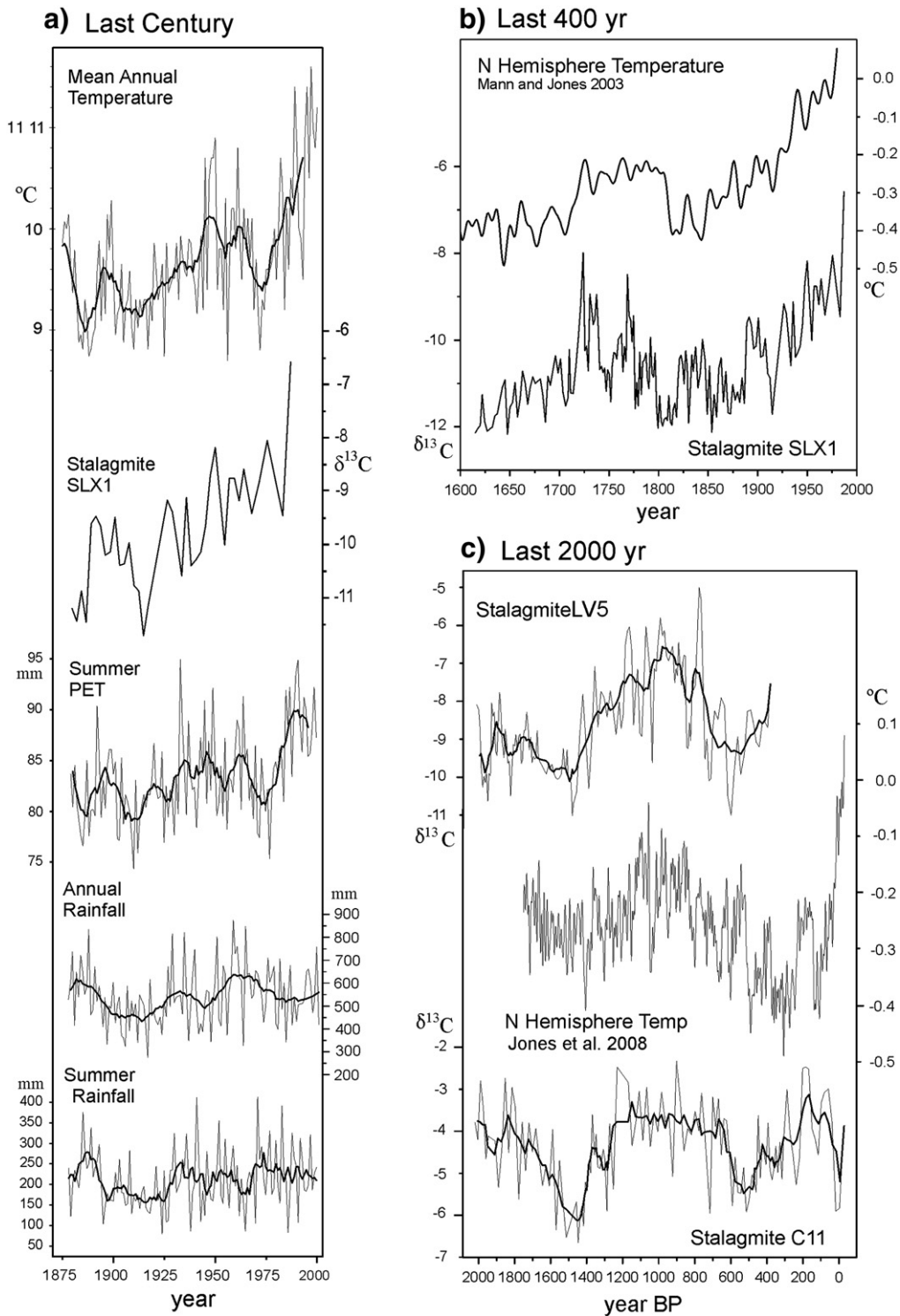


**Fig. 5.** a) Comparison of the  $\delta^{13}\text{C}$  series of stalagmite SLX1 with annual mean temperature, annual and summer rainfall, and summer potential evapotranspiration (PET) series of the Burgos area. Rainfall series come from Burgos-Villafraía Meteorological Station, obtained from the Global Historical Climatology Network (US National Climatic Data Center). The annual mean temperature series are reconstructed from instrumental series from Burgos-Villafraía and Madrid (Agencia Nacional de Meteorología, Spain; Almarza, 2000; Carreras, 2001). The PET series were calculated following the method of Thornthwaite (1948). b) The last 400 years  $\delta^{13}\text{C}$  series of stalagmite SLX1 compared with the reconstructed temperatures for the Northern Hemisphere, according to Mann and Jones (2003). c) The  $\delta^{13}\text{C}$  record of stalagmites LV5 and C11 for the last two millennia compared with reconstructed temperatures for the Northern Hemisphere by Mann et al. (2008).

6.2.  $\delta^{13}\text{C}$  synthetic curve

As suggested by the statistical parameters shown in Table 2, the  $\delta^{13}\text{C}$  in each stalagmite varies within a quite similar range (standard deviation ranging from 0.91 to 1.16) but the absolute values are very different (ranging from  $-4.53$  in C11 to  $-10.28$  in SLX1). As a first

approach, we can assume that the  $\delta^{13}\text{C}$  variability is controlled by environmental changes (i.e., temperature), whereas the absolute averaged values depend on the bulk conditions of each karstic environment. For example, C11 grew in a deep passage of Cueva del Cobre, located  $\sim 100$  m below the surface, where the percolation path can be assumed to be longer, favouring the progressive outgassing of the

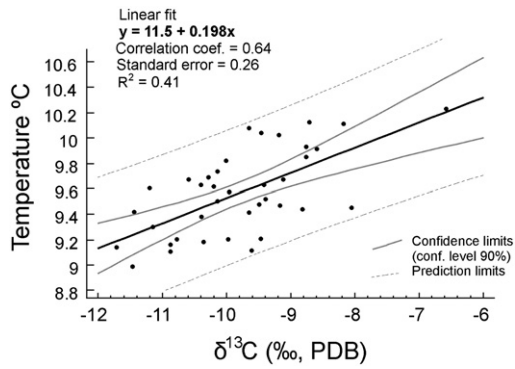


**Fig. 6.** Cross correlation plot between instrumental series of temperatures in Burgos area and  $\delta^{13}\text{C}$  values in stalagmite SLX1 for the time interval 1875–2000. The temperature values are ten-year averages of the annual mean temperatures. See explanation in the text.

percolating waters and the associated enrichment in  $^{13}\text{C}$ . In addition, the lower temperature of water in Cueva del Cobre would have also favoured the interaction of percolating waters with the isotopically heavy marine host limestone, which has  $\delta^{13}\text{C}$  values of about 3.5–4.5‰. In the opposite extreme, stalagmite SLX1, which displays the most depleted  $\delta^{13}\text{C}$  values, grew from drip waters that were warmer, percolated through shorter paths, and dissolved a slightly lighter Cretaceous bedrock ( $\delta^{13}\text{C} = -1.5$ – $2$ ‰).

Assuming that changes of  $\delta^{13}\text{C}$  in each stalagmite depend on external factors such as temperature, but that the karstic conditions determine the bulk mean value, a synthetic time series of relative  $\delta^{13}\text{C}$  values based on the three stalagmites has been constructed in order to provide a continuous record of paleoclimate for the last 4000 years (Fig. 7). This synthetic curve is based on the difference of each  $\delta^{13}\text{C}$  value with the average  $\delta^{13}\text{C}$  value of its stalagmite for the time interval between 1570 and 670 yr BP (the longest interval of continuous and simultaneous growing of the three stalagmites). A smoothing curve based on adjacent averaging ( $n = 25$ ) is also included. It is based on the stacked relative  $\delta^{13}\text{C}$  values of the three stalagmites. This latter curve, which gives a general idea of the broad  $\delta^{13}\text{C}$  changes through the four millennia, should be however considered as tentative, as the density of data per time unit in the three stalagmites is often different enough to determine that each stalagmite record has a quite different relative weight in the final smoothed curve.

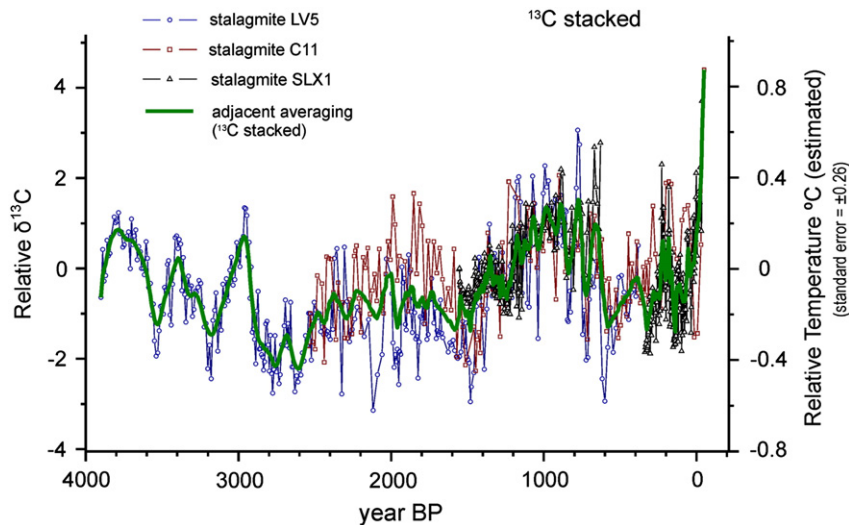


**Fig. 7.** Synthetic time series of relative  $\delta^{13}\text{C}$  values for the last 4000 years, based on the three stalagmites. The curve is based on the deviation of each  $\delta^{13}\text{C}$  value from the mean calculated in each stalagmite for the 1570–670 yr BP interval (i.e., the longest interval of coeval growth in the three samples). The smoothing curve is based on adjacent averaging ( $n = 10$ ) of the stacked relative  $\delta^{13}\text{C}$  values of the three stalagmites. The temperature scale is based on the linear model correlation obtained from the cross-plot of Fig. 6. According to that model, the error of the temperature estimates is  $\pm 0.26$  °C.

An estimate of relative land temperature change in the study area has been also included in Fig. 7. It is based on transfer function deduced from the cross-plot of Fig. 6.

## 7. Discussion

### 7.1. Relation speleothem $\delta^{13}\text{C}$ – surface temperature

The positive correlation between  $\delta^{13}\text{C}$  series of the stalagmites and the surface temperature series shown in the previous section is robust in the three samples, but requires some further discussion. The basic question that arises is about the mechanism capable of inducing the observed direct association speleothem  $\delta^{13}\text{C}$ –surface temperature. Changes in stalagmite  $\delta^{13}\text{C}$  through time may be caused by a number of factors, including: (1) changes in the atmospheric  $\text{CO}_2$  isotopic composition, as those induced by anthropogenic burning of fossil fuels (e.g., Suess, 1955; Genty and Massault, 1999; Genty et al., 2001a; McCarroll and Loader, 2006); (2) changes in the ratio of C3:C4 plants in the overlying vegetation leading to changes in  $\delta^{13}\text{C}$  of soil  $\text{CO}_2$  (e.g., Dorale et al., 1992, 1998; Bar-Matthews et al., 1996; Hopley et al., 2007); (3) changes in vegetation density above the cave (e.g., Amundson et al., 1988; Baldini et al., 2005); (4) degree of mixing between atmospheric  $\text{CO}_2$  and biological  $\text{CO}_2$  derived from root respiration and microbial activity (Baker et al., 1997; Genty and Massault, 1999; Genty et al., 2003); (5) changes in the degree of open versus closed system dissolution of the host limestone by percolating groundwaters above the cave (Hendy, 1971; Salomons and Mook, 1986; Dulinski and Rozanski, 1990); (6) variation in the amount of  $\text{CO}_2$  degassing of drip waters due to changes in air  $p\text{CO}_2$  within the cave (Spötl et al., 2005; Baldini et al., 2008; Matthey et al., 2008); and (7) changes in the amount of prior calcite precipitation, in the roof of the cave and/or elsewhere in the aquifer system (e.g., Verheyden et al., 2000; Tooth and Fairchild, 2003; Johnson et al., 2006; Matthey et al., 2008).

The influence of some of these mechanisms in the studied  $\delta^{13}\text{C}$  speleothem records can be *a priori* discarded because of the characteristics of the studied karst systems. This is the case of the ratio of C3:C4 vegetation: today climatic conditions restrict a significant growth of C4 vegetation, and this restriction must have also occurred during the last millennia (e.g., Cerling, 1997). It is also the case of the atmospheric  $\text{CO}_2$  isotopic composition, as the  $\delta^{13}\text{C}$  of the atmospheric  $\text{CO}_2$  has been very stable through the last millennia (Elsig et al., 2009) with the exception of the last century, when it decreased rapidly as a consequence of fossil fuel

combustion in the atmosphere (e.g., Marino and McElroy, 1991). However, the speleothem  $\delta^{13}\text{C}$  values show major changes through the studied interval and a markedly positive trend for the 20th century, opposite to what should be expected if the so-called 'Suess effect' were relevant. We can also discard mechanisms 3 (vegetation density), 4 (atmospheric  $\text{CO}_2$  input), and probably also 5 (open vs. closed system dissolution), which usually induce depleted  $\delta^{13}\text{C}$  values when increasing temperature, or respond relevantly to rainfall variability, a correspondence that has not been observed in the records. It should be noted, however, that under some particular climatic circumstances, an increase in air temperature could reduce soil moisture above the cave sites, which in turn could lead to a reduction in vegetation density and soil productivity, potentially causing an increase in  $\delta^{13}\text{C}$  values.

Monitoring of modern Kaité cave system (stalagmite LV5) since 2002 reveals that dripping varies seasonally and inter-annually but remains always active, even during the driest periods, allowing calcite to grow continuously as well. Since the site is characterized by a stable cave climate (Turrero et al., 2004; Martín-Chivelet et al., 2006), processes along the vadose-water flow path up to the drip site should be crucial to understand further speleothem  $\delta^{13}\text{C}$  variability. Indeed, there is an inter-annual trend of calcium depletion in the drip water (Turrero et al., 2007), fitting the warm temperatures (heat-wave) registered in central-south Europe from 2003 through 2006, which is superimposed to the intra-annual seasonal trend. Hence, ion pairs in the caves (Mg/Ca, Sr/Ca and Ba/Ca) exhibit a strong correlation with variations in  $\text{Ca}^{2+}$  ( $R^2 > 0.75$ ). Both facts, are interpreted as calcium consumption by prior calcite precipitation, that should induce a  $^{13}\text{C}$ -enriched  $\text{HCO}_3^-$  drip water. A number of studies (e.g. Dreybrodt, 1988; Fairchild et al., 2001; Genty et al., 2001b; Oster et al., 2010) demonstrated that when drip rates are high enough, the main control on speleothem growth could be the mean annual temperature outside the caves, due to the correlation that exists between calcium ion concentration in drip water, soil  $\text{pCO}_2$ , and surface temperature. The variability of the  $\delta^{13}\text{C}$  speleothem time series in relation with temperature can be thus interpreted as the result of the combined effects of secular changes in air  $\text{pCO}_2$  within the caves, and variations in the prior precipitation of calcium carbonate in the flow path through the aquifer system. These mechanisms would explain the positive trends showed by  $\delta^{13}\text{C}$  speleothem during the time intervals of atmospheric warming, and the opposite trends during cooling periods.  $\text{CO}_2$  increased degasification of waters during warm intervals would explain the observed relation.

## 7.2. Implications for climate variability

Thus, if the broad conditions of the studied karst systems (i.e., above the caves, through the flow path, and inside the caves) have not changed substantially during the last four millennia, the medium and long-term variability of the  $\delta^{13}\text{C}$  records can be read in terms of secular changes in regional surface temperature. This leads to the following deductions about past and present climate change:

The surface temperature varied notably in the northern part of inland Spain during the last four millennia, with alternating cold and warm periods. Changes in temperature through time followed weak cyclic patterns, with periodicities of ~1300, 900, and 440 yr. These cycles are broadly comparable to those recognized in other Holocene paleoclimate records and commonly attributed to medium and long-term variations in solar flux and changes in the North Atlantic circulation.

In particular, the 1300 yr cycle could correspond to the 1500 yr cycle recognized for the Holocene in the drift ice sediment record of North Atlantic deep-sea cores (e.g., Bond et al., 1997, 2001; Campbell et al., 1998; Bianchi and McCave, 1999). In fact, the length of the cycles defined by the ice-rafted debris (IRD) is rather variable, and for the last four millennia approaches to 1300 yr. It should be noted that the IRD curves by Bond et al. (2001) show maximum values (i.e. cooler episodes) at 3300, 2700, 1500, 1200, and 400 yr BP, all of them coincident with phases of temperature minima recognized in the stalagmites.

The 900 yr cycle of the speleothems would match the 950 yr cycle recognized in ice cores of Greenland (e.g., O'Brien et al., 1995) and also the 900 yr cycle of the North Atlantic proposed by Schulz and Paul (2002). Finally the 400 yr cycle could be similar to those recognized in both marine (e.g., Bond et al., 2001) and lake records (e.g., Yu and Ito, 2002; Wu et al., 2009) for the middle-late Holocene.

By comparing the temperature changes measured in the area for the last 135 years with the most recent record of the speleothems, we conclude that temperature changes that took place in the study area in the last four millennia occurred within a range of 1.6 °C. The recognized variability is in broad agreement with some reconstructions based on models and other proxies (e.g., Davis et al., 2003).

The  $\delta^{13}\text{C}$  record for the last four millennia defines an initial interval of broad warm conditions between 4000 and 3000 yr BP. It is punctuated by a well-marked cyclicity of 400 yr, defined by three successive cycles of very similar amplitude (Figs. 3 and 7). The thermal minima of these cycles correspond to short, cool intervals, herein dated at ~3950, ~3550, and ~3250 yr BP. Interestingly, this initial warm interval is modulated by a weak and long-term trend towards cooler conditions, indicative of slow and progressive climate deterioration, superposed to the higher frequency 400 yr cycles.

The slow progressive deterioration rapidly accelerates since ~2900 yr BP and derived in a prolonged time during which thermal conditions become permanently cold and the ~400 yr cyclicity appears notably masked. The coldest conditions occurred during 300 years (2850–2550 yr BP), an interval that can be correlated with the "first cold phase" of the Subatlantic period, also called in Europe the Iron Age Cold Period. This period has been recognized by Desprat et al. (2003) in sediments from the Ría de Vigo in the northwestern coast of Spain, and has been also reported from different areas and proxies in central and western Europe (e.g., van Geel et al., 1996; Speranza et al., 2002; Blaauw et al., 2004; Plunkett and Swindles, 2008), and Greenland (O'Brien et al., 1995). The onset of this episode is essentially concurrent with the minimum in the solar activity ( $\Delta^{14}\text{C}$  maximum) that took place at ~2800 yr BP (e.g., Swindles et al., 2007; Usoskin et al., 2007). Also, it can be correlated with a period of generalized cooling in central Europe (e.g., van Geel et al., 1996) the IRD event 2 (~2700 yr BP) of the Atlantic cores (Bond et al., 1997, 2001) and with a major perturbation in the deep North Atlantic (~2700 yr BP) interpreted as the main weakening of Iceland–Scotland Overflow Waters (ISOW) for the Holocene (Hall et al., 2004).

The cold interval ended around 2500 yr BP, when a gradual amelioration trend leads the onset of a relatively warmer interval which would last until ~1700 yr BP. This new interval, warmer than the previous one, never reached the high temperatures of the 4000–3000 yr BP initial interval. It should be noted that the warm interval was particularly well recorded in stalagmite C11, and more tenuously in LV5, where the signal is noisier. Maximum temperatures were probably reached in the three hundred years interval between 2150 yr BP and 1750 yr BP. That smooth "optimum", should correspond to the well-known Roman Warm Period (e.g., Lamb, 1985), an interval which has been correlated with a phase of relatively high solar flux (e.g., Bond et al., 2001; Usoskin et al., 2007). Interestingly, the Roman Warm Period appears in the stalagmite LV5 record punctuated by a short, small temperature minimum at ~2140 yr BP, which could be related with the solar minima recorded at 2300 yr BP (Usoskin et al., 2007).

After those relatively warm centuries of the Roman Warm Period, a progressive diminution of surface temperature took place again in the area, leading to another relatively cold episode, which lasted about 250 years and reaches its minimum at ~1500 yr BP. This cold interval (and its thermal minimum) is well defined in the three stalagmites, and correlates with the Dark Ages Cold Period described in other areas of Europe including some points of Iberia (Gil-García et al., 2007). This episode is concurrent with the IRD event 1 of the Atlantic cores (Bond et al., 2001) and with a period of markedly low temperatures in the Sargasso Sea (e.g., Keigwin, 1996).

The Dark Ages Cold Period is relatively short, and after the 1500 yr BP minimum, a rapid trend of warming led to a new, prolonged interval of warmth, which is attributed to the Medieval Warm Period. This interval lasted from 1400 yr BP until 700 yr BP, although punctuated by at least two minor, relatively cold events, which took place at ~1250 and ~850 yr BP. The Medieval Warm Period is probably the most robust climatic feature in our records, perfectly outlined in the series of the three stalagmites. It has a similar duration but is warmer than the Roman Warm Period. This aspect is in agreement with previous studies in Northern and Central Spain (Martínez-Cortizas et al., 1999; Gil-García et al., 2007). Temperatures during the Medieval Warm Period were also warmer than in the 4000–3000 yr BP initial interval.

The end of the Medieval Warm Period was marked by a progressive and rapid decrease in temperature, which is well defined in two of the stalagmites (LV5 and C11) whereas the third one interestingly stopped its growth when the rapid cooling began. That deterioration interval marks the rapid transition into the Little Ice Age, a relatively cold period broadly reported from all Europe (e.g., Lamb, 1977; Fagan, 2000) and also from other areas in the world as far as South Africa or South America (e.g., Holmgren et al., 2001; Meyer and Wagner, 2009) and whose cause, still debated, could be a combination of low solar activity (e.g., Lean et al., 1995; Usoskin et al., 2003), changes in thermohaline circulation (e.g., Broecker, 2000) and other factors such as increased explosive volcanism (e.g., Robock, 1979; Crowley, 2000) and anthropogenic changes in forestation (Ruddiman, 2003). In our record, this cold period started at 750 yr BP and lasted until the second half of the 19th century, although a slight amelioration can be observed from 250 yr BP onwards. The coldest conditions of this broadly cold interval were reached during three short periods, dated respectively 600–500 yr BP, 350–300 yr BP, and 150–100 yr BP. From these, the two former seem to be more intense than the third one.

Interestingly, after the second cold event of the Little Ice Age, stalagmite SLX1 resumed its growth until our days. The interpretation of the record of this stalagmite for these last 400 years indicates a net increase of temperature, which correlates well with the hemispheric reconstructions of temperature (e.g., Mann and Jones, 2003; Mann et al., 2008). However, it should be noted that the range of temperature change obtained in this paper for inland Northern Spain is about two times greater than the range proposed for the Northern Hemisphere temperature in average.

Despite the variability of temperature recognized for the last four millennia, the warming that occurred during the last century seems to be fastest and more intense than any previous one recognized in the studied speleothems. Also, the temperatures of the end of the 20th century are the highest of the whole interval. This is in clear disagreement with some studies in Northern Spain based on peat bog proxies, which suggest that the temperatures during both the Roman Warm Period and the Medieval Warm Period were higher than present-day ones (Martínez-Cortizas et al., 1999). This apparent contradiction could be related to the difficulty for recognizing the very fast warming interval of the second half of the 20th century in the relatively lower-resolution sedimentary record of wetlands.

## 8. Conclusions

The  $\delta^{13}\text{C}$  series of three stalagmites provide a 4000 year regional record of relative temperature in inland northern Spain which reflects variability at decadal to millennial scales in the range of  $\pm 0.8$  °C. As expected in mid-latitude continental areas, this area in Spain is highly sensitive to climate change. That variability follows significant cycles with periodicities of ~1300, ~900 and ~400 yr, in agreement with those recognized in the North Atlantic deep marine cores and the Greenland ice cores, as well as some other terrestrial records of the middle – late Holocene, suggesting common forcing mechanisms.

The  $\delta^{13}\text{C}$  variability reasonably replicates the surface temperature changes of the available regional instrumental series. Also,  $\delta^{13}\text{C}$  patterns

correlate well with Northern Hemisphere temperature reconstructed series for the last four centuries and also for the last 1000 years. Covariation of the land surface temperature in northern Spain with temperature anomalies from the North and the Central Atlantic and the Greenland ice cores suggest that the variability at multidecadal to centennial time scales in the speleothem records reflects a high sensitivity of the continental area to changes in solar radiance and also to changes in the North Atlantic circulation patterns that occurred during the middle and late Holocene.

The  $\delta^{13}\text{C}$  record for the last four millennia shows alternating colder and warmer intervals, whose timing and duration have been precisely constrained by  $^{230}\text{Th}$  radiometric dating. Main climatic periods are: (1) 3950–3000 yr BP: warm period punctuated by cool events around ~3950, 3550 and 3250 yr BP, and characterized by a marked 0.4 ky cyclicity; (2) 2850–2500 yr BP: cold interval (Iron Age Cold Period), coincident with a solar activity minimum and with a major perturbation in the North Atlantic circulation; (3) 2500–1650 yr. BP: interval of moderate warmth (Roman Warm Period), with maximum temperatures between 2150 and 1750 yr BP; (4) 1650–1400 yr BP: short cold interval (Dark Ages Cold Period), with a thermal minimum at ~1500 yr BP.; (5) 1400–700 yr BP: long warm period (Medieval Warm Period), punctuated by at least two minor, cooler events (~1250 and ~850 yr BP); (6) 700–100 yr BP: Broad cold period (Little Ice Age), in which the coldest conditions occurred at 600–500 yr BP, 350–300 yr BP, and 150–100 yr BP; and (7) Last 150 years: Rapid warming interval which leads to the highest temperatures of the last four millennia. Transitions between successive intervals are usually progressive but rapid (lasting about one or two centuries), although the “modern warming” is fastest than any previous transition.

The speleothem records show a notable variability of land temperature in northern inland Spain, with robust signatures of alternating warmer and colder intervals at centennial to millennial scales. Within this framework of change, the present “modern warming” appears as a singular feature because of its rapidity and intensity.

Finally, we emphasize the potential of speleothem  $\delta^{13}\text{C}$  in paleoclimatology. Difficult to interpret and calibrate as it is, it can show a high sensibility to climate or environmental change. Further research is necessary for a better profiting of this often forgotten proxy.

## Acknowledgements

The work was carried out with the support of the following projects and grants: PR-2007-0111, PR-2007-0197, CGL2007-60618-BTE, and CGL2010-21499-BTE. We greatly thank the facilities and permissions given by the Junta de Castilla y León (Spain) for accessing and working in the Ojo Guareña Natural Monument and World Heritage Site, Atapuerca World Heritage Site, and the Fuentes Carrionas-Fuente Cobre Natural Park. The authors specially thank Dr. C. Rossi (Univ. Complutense de Madrid) for his contribution in the early stages of this project, Dr. X. Wang (Columbia University) for priceless advice and help during the U/Th analytical work, Dr. J.L. Arsuaga for his inestimable support in Atapuerca, Ms. Maniko Solheid (Minnesota Isotope Laboratory) for  $^{13}\text{C}$  analyses, and Dr. J.M. Gómez Ros (Ciemat) for his help with statistics. The collaborations of Mr. M.A. Martín-Merino (Grupo Espeleológico Edelweiss, Burgos) during cave work, and of Mr. G. Herrero (Univ. Complutense de Madrid), for sample preparation, are also greatly appreciated. Thanks are extended to all participants of CLISP and CLISP2 projects. Finally, the comments and suggestions on the paper by two anonymous referees and Editor H. Oberhänsli are sincerely acknowledged.

## References

- Almaraz, C., 2000. Respuesta al Calentamiento Global de la serie de temperatura media anual de Madrid. Actas de la II Asamblea Hispano-Lusa de Geodesia y Geofísica, Lagos (Portugal).

- Amundson, R.G., Chadwick, O.A., Sowers, J.M., Doner, H.E., 1988. Relationship between climate and vegetation and the stable carbon isotope chemistry of soils in the eastern Mojave Desert, Nevada. *Quaternary Research* 29 (3), 245–254.
- Baker, A., Ito, E., Smart, P.L., McEwan, R.F., 1997. Elevated and variable values of  $^{13}\text{C}$  in speleothems in a British cave system. *Chemical Geology* 136, 263–270.
- Baldini, J.U.L., McDermott, F., Baker, A., Baldini, L.M., Matthey, D.P., Railsback, L.B., 2005. Biomass effects on stalagmite growth and isotope ratios: a 20th century analogue from Wiltshire, England. *Earth and Planetary Science Letters* 240 (2), 486–494.
- Baldini, J.U.L., McDermott, F., Hoffmann, D.L., Richards, D.A., Clipson, N., 2008. Very high-frequency and seasonal cave atmosphere  $\text{P-CO}_2$  variability: implications for stalagmite growth and oxygen isotope-based paleoclimate records. *Earth and Planetary Science Letters* 272, 118–129.
- Bar-Matthews, M., Ayalon, A., Matthews, A., Sass, E., Halicz, L., 1996. Carbon and oxygen isotope study of the active water-carbonate system in a karstic Mediterranean cave: implications for paleoclimate research in semiarid regions. *Geochimica et Cosmochimica Acta* 60 (2), 337–347.
- Bianchi, G.G., McCave, I.N., 1999. Holocene periodicity in North Atlantic climate and deep-ocean flow south of Iceland. *Nature* 397, 515–517.
- Blaauw, M., Blaauw, M., van Geel, B., van der Plicht, J., 2004. Solar forcing of climate change during the mid-Holocene: indications from raised bogs in The Netherlands. *Holocene* 14 (1), 35–44.
- Bond, G., Showers, W., Cheseby, M., Lotti, R., Almasi, P., deMenocal, P., Priore, P., Cullen, H., Hajdas, I., Bonani, G., 1997. A pervasive millennial-scale cycle in North Atlantic Holocene and glacial climates. *Science* 278, 1257–1266.
- Bond, G., Kromer, B., Beer, J., Muscheler, R., Evans, M.N., Showers, W., Hoffmann, S., Lotti-Bond, R., Hajdas, I., Bonani, G., 2001. Persistent solar influence on North Atlantic climate during the Holocene. *Science* 294, 2130–2136.
- Broecker, W.S., 2000. Was a change in thermohaline circulation responsible for the Little Ice Age? *Proceeding of the National Academy of Sciences* 97 (4), 1339–1342.
- Campbell, I.D., Campbell, C., Apps, M.J., Rutter, M.W., Bush, A.B.G., 1998. Late Holocene. 1500 year climatic periodicities and their implications. *Geology* 26, 471–473.
- Carreras, L., 2001. Influencia de la actividad volcánica explosiva mundial sobre los registros de temperatura de Madrid (1860–2001). Tesis de Master. Instituto Nacional de Meteorología - Universidad Complutense de Madrid (Unpublished).
- Cerling, T.E., 1997. Late Cenozoic vegetation change, atmospheric  $\text{CO}_2$ , and tectonics. In: Rudimann, W.M. (Ed.), *Uplift and Climate Change*. Plenum Press, New York, pp. 313–327.
- Cheng, H., Edwards, R.L., Hoff, J., Gallup, C.D., Richards, D.A., Asmerom, Y., 2000. The half-lives of uranium-234 and thorium-230. *Chemical Geology* 169, 17–33.
- Christensen, J.H., Hewitson, B., Busuioc, A., Chen, A., Gao, X., Held, I., Jones, R., Kolli, R.K., Kwon, W.-T., Laprise, R., Magaña Rueda, V., Mearns, L., Menéndez, C.G., Räisänen, J., Rinke, A., Sarr, A., Whetton, P., 2007. Regional Climate Projections. In: Solomon, S., Qin, D., Manning, M., Chen, Z., Marquis, M., Averyt, K.B., Tignor, M., Miller, H.L. (Eds.), *Climate Change 2007: The Physical Science Basis*. Contribution of Working Group I to the Fourth Assessment Report of the Intergovernmental Panel on Climate Change. Cambridge University Press, Cambridge and New York.
- Crowley, T.J., 2000. Causes of climate change over the past 1000 years. *Science* 289 (5477), 270–277.
- Davis, B.A.S., Brewer, S., Stevenson, A.C., Guiot, J., 2003. The temperature of Europe during the Holocene reconstructed from pollen data. *Quaternary Science Reviews* 22, 1701–1716.
- Desprat, S., Sánchez-Goni, M.F., Loutre, M.-F., 2003. Revealing climatic variability of the last three millennia in northwestern Iberia using pollen influx data. *Earth and Planetary Science Letters* 213, 63–78.
- Domínguez-Villar, D., Martín-Chivelet, J., Edwards, R.L., 2004. Laminación anual en un espeleotema del Holoceno Inferior (Cueva de Kaite, Complejo Kárstico de Ojo Guareña, Burgos). *Implicaciones paleoclimáticas*. *Geo-Temas* 6 (5), 89–92.
- Domínguez-Villar, D., Wang, X., Cheng, H., Martín-Chivelet, J., Edwards, R.L., 2008. A high-resolution late Holocene Speleothem record from Kaite cave, Northern Spain:  $\delta^{18}\text{O}$  variability and possible causes. *Quaternary International* 187, 40–51.
- Dorale, J.A., González, L.A., Reagan, M.K., Pickett, D.A., Murrell, M.T., Baker, R.G., 1992. A high-resolution record of Holocene climate change in speleothem calcite from Cold Water Cave, Northeast Iowa. *Science* 258, 1626–1630.
- Dorale, J.A., Edwards, R.L., Ito, E., González, L.A., 1998. Climate and vegetation history of the midcontinent from 75 to 25 ka: a speleothem record from Crevice Cave, Missouri, USA. *Science* 282, 1871–1874.
- Dorale, J.A., Edwards, R.L., Alexander, E.C., Shen, C.-C., Richards, D.A., Cheng, H., 2004. Uranium-series dating of speleothems: current techniques, limits and applications. In: Sasowsky, I.D., Mylroie, J. (Eds.), *Studies of Cave Sediments. Physical and Chemical Records of Palaeoclimate*. Kluwer Academic, New York, pp. 177–197.
- Dreybrodt, W., 1988. Processes in Karst systems. *Physics, chemistry and geology*. Springer Series in Physical Environment 4. Springer-Verlag, New York. 288 pp.
- Dulinski, M., Rozanski, K., 1990. Formation of  $^{13}\text{C}/^{12}\text{C}$  isotope ratios in speleothems: a semi-dynamic model. *Radiocarbon* 32, 7–16.
- Edwards, R.L., Chen, J.H., Wasserburg, G.J., 1987.  $^{238}\text{U}$ – $^{234}\text{U}$ – $^{230}\text{Th}$ – $^{232}\text{Th}$  systematics and the precise measurement of time over the past 500,000 y. *Earth and Planetary Science Letters* 81, 175–192.
- Elsig, J., Schmitt, J., Leuenberger, D., Schneider, R., Eyer, M., Leuenberger, M., Joos, F., Fischer, H., Stocker, T.F., 2009. Stable isotope constraints on Holocene carbon cycle changes from an Antarctic ice core. *Nature* 461, 507–510.
- Fagan, B., 2000. *The Little Ice Age: How Climate Made History, 1300–1850*. Basic Books, New York. 246 pp.
- Fairchild, I.J., Baker, A., Borsato, A., Frisia, S., Hinton, R.W., McDermott, F., Tooth, A.F., 2001. Annual to sub-annual resolution of multiple trace-element trends in speleothems. *Journal of the Geological Society of London* 158, 831–841.
- Fairchild, I.J., Smith, C.L., Baker, A., Fuller, L., Spötl, C., Matthey, D., McDermott, F., E.I.M.F., 2006. Modification and preservation of environmental signals in speleothems. *Earth Science Reviews* 75, 105–153.
- Frisia, S., Borsato, A., Fairchild, I.J., McDermott, F., 2000. Calcite fabrics, growth mechanisms, and environment of formation in speleothems from the Italian Alps and southwestern Ireland. *Journal of Sedimentary Research* 70, 1183–1196.
- Genty, D., Massault, M., 1999. Carbon transfer dynamics from bomb- $^{14}\text{C}$  and  $\delta^{13}\text{C}$  time series of a laminated stalagmite from SW France—modelling and comparison with other stalagmite records. *Geochimica et Cosmochimica Acta* 63, 1537–1548.
- Genty, D., Baker, A., Massault, M., Proctor, C., Gilmour, M., Pons-Branchu, E., Hamelin, B., 2001a. Dead carbon in stalagmites: carbonate bedrock palaeodissolution vs. ageing of soil organic matter. Implications for  $^{13}\text{C}$  variations in speleothems. *Geochimica et Cosmochimica Acta* 65, 3443–3457.
- Genty, D., Baker, A., Vokal, B., 2001b. Intra- and inter-annual growth rate of modern stalagmites. *Chemical Geology* 176, 191–212.
- Genty, D., Blamart, D., Ouahdi, R., Gilmour, M., Baker, A., Jouzel, J., Van-Exer, S., 2003. Precise dating of Dansgaard-Oeschger climate oscillations in western Europe from stalagmite data. *Nature* 421, 833–838.
- Gil-García, M.J., Ruiz-Zapata, M.B., Santisteban, J.L., Mediavilla, R., López-Pamo, E., Dabrio, C.J., 2007. Late Holocene environments in Las Tablas de Daimiel (south central Iberian Peninsula, Spain). *Vegetation History and Archaeobotany* 16, 241–250.
- Hall, I.R., Bianchi, G.G., Evans, J.R., 2004. Centennial to millennial scale Holocene climate-deep water linkage in the North Atlantic. *Quaternary Science Reviews* 23, 1529–1536.
- Hammer, Ø., Harper, D.A.T., Ryan, P.D., 2003. *PAST—Palaeontological Statistics*, ver. 1.58. <http://folk.uio.no/ohammer/past>.
- Hendy, C.H., 1971. The isotopic geochemistry of speleothems: I. The calculation of the effects of different modes of formation on the isotopic composition of speleothems and their applicability as palaeoclimatic indicators. *Geochimica et Cosmochimica Acta* 35, 801–824.
- Holmgren, K., Tyson, P.D., Moberg, A., Svanered, O., 2001. A preliminary 3000-year regional temperature reconstruction for South Africa. *South African Journal of Science* 97, 49–51.
- Hopley, P.J., Marshall, J.D., Weedon, G.P., Latham, A.G., Herries, A.I.R., Kuykendall, K.L., 2007. Orbital forcing and the spread of C4 grasses in the late Neogene: stable isotope evidence from South African speleothems. *Journal of Human Evolution* 53, 620–634.
- Johnson, K.R., Hu, C.Y., Belshaw, N.S., Henderson, G.M., 2006. Seasonal trace-element and stable-isotope variations in a Chinese speleothem: the potential for high-resolution paleomonsoon reconstruction. *Earth and Planetary Science Letters* 244, 394–407.
- Keigwin, L.D., 1996. The Little Ice Age and Medieval Warm Period in the Sargasso Sea. *Science* 274, 1504–1508.
- Kjellström, E., Bärring, L., Jacob, D., Jones, R., Lenderink, G., Schär, C., 2007. Modelling daily temperature extremes: recent climate and future changes over Europe. *Climatic Change* 81, 249–265.
- Lamb, H.H., 1977. *Climate: Present, Past and Future, Volume 2: Climatic History and the Future*. Methuen, London. 837 pp.
- Lamb, H.H., 1985. *Climatic History and the Future*. Princeton Univ. Press.
- Lean, J., Beer, J., Bradley, R., 1995. Reconstruction of solar irradiance since 1610: implications for climate change. *Geophysical Research Letters* 22 (23), 3195–3198.
- Mann, M.E., Jones, P.D., 2003. Global surface temperatures over the past two millennia. *Geophysical Research Letters* 30 (15), 1820.
- Mann, M.E., Zhang, Z., Hughes, M.K., Bradley, R.S., Miller, S.K., Rutherford, S., Ni, F., 2008. Proxy-based reconstructions of hemispheric and global surface temperature variations over the past two millennia. *Proceedings of the National Academy of Sciences* 105 (36), 13252–13257.
- Marino, B.D., McElroy, M.B., 1991. Isotopic composition of atmospheric  $\text{CO}_2$  inferred from carbon in C4 plant cellulose. *Nature* 349, 127–131.
- Martín-Chivelet, J., Muñoz, B., Domínguez Villar, D., Turrero, M.J., Ortega, A.I., 2006. Comparative analysis of stalagmites from two caves of Northern Spain. Implications for Holocene paleoclimate studies. *Geologica Belgica* 9 (3/4), 323–335.
- Martín-Chivelet, J., Muñoz-García, M.B., Turrero, M.J., Ortega, A.I., Domínguez-Villar, D., 2008. 4000 years of climate change in Northern Spain from speleothem records. *Geochimica et Cosmochimica Acta* 71 (15–1), A597.
- Martín-Chivelet, J., Turrero, M.J., Garralón, A., Gómez, P., Muñoz-García, M.B., Sánchez, L., Santisteban, J.I., 2009. Modeling  $\delta^{18}\text{O}$  in drip waters and recent speleothems: implications for paleoclimate records in N Spain. *Geochimica et Cosmochimica Acta* 73 (13–1), A840.
- Martínez-Cortizas, A., Pontevedra-Pombal, X., García-Rodeja, E., Novoa-Muñoz, J.C., Shoyk, W., 1999. Mercury in a Spanish peat bog: archive of climate change and atmospheric metal deposition. *Science* 284, 939–942.
- Martín-Merino, M.A., 1986. Descripción preliminar del karst de Ojo Guareña. *Kaite* 4–5, 53–72.
- Matthey, D., Lowry, D., Duffet, J., Fisher, R., Hodge, E., Frisia, S., 2008. A 53 year seasonally resolved oxygen and carbon isotope record from a modern Gibraltar speleothem: reconstructed drip water and relationship to local precipitation. *Earth and Planetary Science Letters* 269, 80–95.
- McCarroll, D., Loader, N.J., 2006. Isotopes in tree rings. In: Leng, M.J. (Ed.), *Isotopes in Palaeoenvironmental Research, Developments in Palaeoenvironmental Research Series*. Springer, Dordrecht, The Netherlands, pp. 67–115.
- McDermott, F., 2004. Palaeoclimate reconstruction from stable isotope variations in speleothems: a review. *Quaternary Science Reviews* 23, 901–918.
- McDermott, F., Schwarcz, H.P., Rowe, P.J., 2006. Isotopes in speleothems. In: Leng, M.J. (Ed.), *Isotopes in Palaeoenvironmental Research, Developments in Palaeoenvironmental Research Series*. Springer, Dordrecht, The Netherlands, pp. 185–226.
- Meyer, I., Wagner, S., 2009. The Little Ice Age in Southern South America: proxy and model based evidence. In: Vimeux, F., Sylvestre, F., Khodri, M. (Eds.), *Past climate variability in south america and surrounding regions*. From the Last Glacial

- Maximum to the Holocene: Developments in Paleoenvironmental Research, vol. 14, pp. 395–414.
- Moreno, J.M., coord., 2005. Evaluación preliminar de los Impactos en España por Efecto del Cambio Climático. Ministerio de Medio Ambiente, Madrid.
- Muñoz-García, M.B., 2007. Estudio de los espeleotemas recientes de Cueva del Cobre (Palencia) como indicadores de variabilidad paleoclimática. Tesis Doctoral. Universidad Complutense de Madrid, España. (available on line at <http://eprints.ucm.es/7738/1/T29991.pdf>).
- Muñoz-García, M.B., Martín-Chivelet, J., Rossi, C., Ford, D.C., Schwarcz, H.P., 2006. Microstratigraphic logs: a method for improving time correlation of speleothems for paleoclimate studies. In: Onac, B.P., Tamas, T., Constantin, S., Persoiu, A. (Eds.), Archives of climate change in karst, vol. 10. Karst waters Institute Special Publication, pp. 60–63.
- Muñoz-García, M.B., Martín-Chivelet, J., Rossi, C., Ford, D.C., Schwarcz, H.P., 2007. Chronology of Termination II and the Eemian period in Southern Europe based on U–Th dating and stable isotope chronology of stalagmites from Cueva del Cobre (N Spain). *Journal of Iberian Geology* 33 (1), 17–30.
- Muñoz-García, M.B., Ortega, A.I., Martín-Chivelet, J., Turrero, M.J., Arsuaga, J.L., 2009. Evidencias de ocupación humana en Cueva Mayor (Sierra de Atapuerca, Burgos) durante la Edad del Bronce a partir de láminas oscuras en espeleotemas. *Livro de Resumos. VII Reuniao do Quaternário Ibérico*, Faro, pp. 206–209.
- O'Brien, S.R., Mayewski, P.A., Meeker, L.D., Meese, D.A., Twickler, M.S., Whitlow, S.I., 1995. Complexity of Holocene climate as reconstructed from a Greenland ice core. *Science* 270 (5244), 1962–1964.
- Ortega A.I., 2009. Evolución geomorfológica del Karst de la Sierra de Atapuerca (Burgos) y su relación con los yacimientos pleistocenos que contiene. Tesis Doctoral, Universidad de Burgos, España.
- Oster, J.L., Montañez, I.P., Guilderson, T.P., Sharp, W.D., Banner, J.L., 2010. Modelling speleothem  $\delta^{13}\text{C}$  variability in a central Sierra Nevada cave using 14 C and  $^{87}\text{Sr}/^{86}\text{Sr}$ . *Geochimica et Cosmochimica Acta* 74, 5228–5242.
- Plunkett, G., Swindles, G.T., 2008. Determining the Sun's influence on Late Glacial and Holocene climates: a focus on climate response to centennial-scale solar forcing at 2800 cal. BP. *Quaternary Science Reviews* 27 (1–2), 175–184.
- Raso, J.M., 1997. The recent evolution of mean annual temperatures in Spain. In: Martín-Vide, J. (Ed.), *Advances in historical climatology in Spain*. Oikos-tau, Barcelona, pp. 201–223.
- Robock, A., 1979. The "Little Ice Age": Northern Hemisphere average observations and model calculations. *Science* 206 (4425), 1402–1404.
- Rossi, C., Muñoz, A., Cortel, A., 1997. Cave development along the water table in Cobre System (Sierra de Peñalabra, Cantabrian Mountains, N Spain). *Proceedings of the 12th International Congress of Speleology*. La Chaux-de-onds, Switzerland, pp. 179–182.
- Ruddiman, W.F., 2003. The anthropogenic greenhouse era began thousands of years ago. *Climatic Change* 61, 261–293.
- Salomons, W., Mook, W.G., 1986. Isotope geochemistry of carbonates in the weathering zone. In: Fritz, P., Fontes, C.J. (Eds.), *Handbook of Environmental Isotope Geochemistry*. The Terrestrial Environment, B, vol. 2. Elsevier, Amsterdam, pp. 239–270.
- Schulz, M., Paul, A., 2002. Holocene climate variability on centennial-to-millennial time scales: 1. Climate records from the North-Atlantic Realm. In: Wefer, G., Berger, W., Behre, K.-E., Jansen, E. (Eds.), *Climate Development and History of the North Atlantic Realm*. Springer-Verlag, Berlin Heidelberg, pp. 41–54.
- Shen, C., Edwards, R.L., Cheng, H., Dorale, J., Thomas, R.B., Moran, S.B., Weinstein, S.E., Edmonds, H.N., 2002. Uranium and thorium isotopic and concentration measurements by magnetic sector inductively coupled plasma mass spectrometry. *Chemical Geology* 185, 165–178.
- Spencer, A., van Geel, B., van der Plicht, J., 2002. Evidence for solar forcing of climate change at ca. 850 cal BC from a Czech peat sequence. *Global and Planetary Change* 35, 51–65.
- Spötl, C., Fairchild, I.J., Tooth, A.F., 2005. Cave air control on dripwater geochemistry, Obir Caves (Austria): implications for speleothem deposition in dynamically ventilated caves. *Geochimica et Cosmochimica Acta* 69, 2451–2468.
- Suess, H.E., 1955. Radiocarbon concentration in modern wood. *Science* 122 (3166), 415–417.
- Swindles, G.T., Plunkett, G., Roe, H.M., 2007. A delayed climatic response to solar forcing at 2800 cal.BP: multiproxy evidence from three Irish peatlands. *Holocene* 17 (2), 177–182.
- Thorntwaite, C.W., 1948. An approach toward a rational classification of climate. *Geographical Review* 38 (1), 55–94.
- Tooth, A.F., Fairchild, I.J., 2003. Soil and karst aquifer hydrological controls on the geochemical evolution of speleothem-forming drip waters, Crag Cave, southwest Ireland. *Journal of Hydrology* 273, 51–68.
- Turrero, M.J., Garralón, A., Martín-Chivelet, J., Gómez, P., Sánchez, L., Quejido, A., Martín-Merino, M.A., Ortega, A.I., 2004. Seasonal changes in the chemistry of drip waters in Kaité Cave (N Spain). In: Wanty, R.B., Seal II, R.S. (Eds.), *Water–Rock Interaction 11*. Balkema Publishers, London, pp. 1407–1410.
- Turrero, M.J., Garralón, A., Gómez, P., Sánchez, L., Martín-Chivelet, J., Ortega, A.I., 2007. Geochemical evolution of drip-water and present-growing calcite at Kaité cave (N Spain). In: Bullen, T.D., Wang, Y.X. (Eds.), *Water–Rock Interaction 12*. Balkema Publishers, Rotterdam, pp. 1187–1190.
- Turrero, M.J., Martín-Chivelet, J., Garralón, A., Gómez, P., Sánchez, L., Muñoz-García, M.B., Ortega, A.I., 2009.  $\delta^{18}\text{O}$  in drip waters and present-day calcite from Kaité and Cueva Mayor Caves (Spain): clues for paleoenvironmental calibration. 8th International Symposium on Applied Isotope Geochemistry, Quebec, Canada, Program and Abstract Volume, p. 61.
- Usoskin, I.G., Solanki, S.K., Schüssler, M., Mursula, K., Alanko, K., 2003. Millennium-scale sunspot number reconstruction: evidence for an unusually active sun since the 1940s. *Physical Review Letters* 91 (21), 211101–1–211101–4.
- Usoskin, I.G., Solanki, S.K., Kovaltsov, G.A., 2007. Grand minima and maxima of solar activity: new observational constraints. *Astronomy and Astrophysics* 471, 301–309.
- van Geel, B., Buurman, J., Waterbolk, H.T., 1996. Archaeological and palaeoecological indications of an abrupt climate change in The Netherlands, and evidence for climatological teleconnections around 2650 BP. *Journal of Quaternary Science* 11, 451–460.
- Verheyden, S., Keppens, E., Fairchild, I.J., McDermott, F., Weis, D., 2000. Mg, Sr and Sr isotope geochemistry of a Belgian Holocene speleothem: implications for paleoclimate reconstructions. *Chemical Geology* 169, 131–144.
- Wu, J., Yu, Z., Zeng, Z., Wang, N., 2009. Possible solar forcing of 400-year wet–dry climate cycles in northwestern China. *Climatic Change* 96, 473–482.
- Yu, Z.C., Ito, E., 2002. The 400-year wet–dry climate cycle in Interior North America and its solar connection. In: West, G.J., Blomquist, N.L. (Eds.), *Proceedings of the nineteenth annual pacific climate workshop*. Technical Report 71 of the interagency ecological program for the San Francisco estuary, pp. 159–163.